International Journal of Chemical, Materials and Biomolecular Sciences
ISSN: 2415-6620
Vol:4, No:2, 2010

Current Distribution and Cathode Flooding Prediction in a PEM Fuel Cell

A. Jamekhorshid, G. Karimi, I. Noshadi, A. Jahangiri

***Abstract*—**Non-uniform current distribution in polymer electrolyte membrane fuel cells results in local over-heating, accelerated ageing, and lower power output than expected. This issue is very critical when fuel cell experiences water flooding. In this work, the performance of a PEM fuel cell is investigated under cathode flooding conditions. Two-dimensional partially flooded GDL models based on the conservation laws and electrochemical relations are proposed to study local current density distributions along flow fields over a wide range of cell operating conditions. The model results show a direct association between cathode inlet humidity increases and that of average current density but the system becomes more sensitive to flooding. The anode inlet relative humidity shows a similar effect. Operating the cell at higher temperatures would lead to higher average current densities and the chance of system being flooded is reduced. In addition, higher cathode stoichiometries prevent system flooding but the average current density remains almost constant. The higher anode stoichiometry leads to higher average current density and higher sensitivity to cathode flooding.

***Keywords*—**Current distribution, Flooding, Hydrogen energy system, PEM fuel cell.

I. Introduction

THERE are two key problems with continued use of fossil fuels, which meet about 80% of the world energy demand today. The first problem is that they are limited in amount and sooner or later will be depleted. The second is that fossil fuels are causing serious environmental problems. Early in the 1970s Hydrogen Energy System had been proposed as a solution for these two interconnected global problems [1]. Hydrogen is an excellent energy carrier with many unique properties. One of its unique properties is that through electrochemical processes, it can be converted to electricity in fuel cells.

Fuel cells are electrochemical devices that convert chemical energy of reactants into electrical energy directly. In particular, polymer electrolyte membrane or proton exchange membrane (PEM) fuel cells have desirable properties. Owing to many advantages associated with them, such as non-pollution, high efficiency, quick startup, and low noise, they are widely regarded as an alternative power source for stationary co-generation units, automotive and portable applications [2].

A significant amount of research has been devoted to the development of PEM fuel cells technologies over the past few years; however, there are still major challenges which need to be overcome, especially in prolonging the lifetime of the PEM fuel cells [3]. One such issue is non-uniform current distribution within the cell which results in local over-heating, accelerated ageing and lower power output than expected [4-6].

The local current distribution in a PEM fuel cell depends on many factors, such as non-uniform loading of catalyst layers, non-uniform feed supply over the cell surface, partial flooding of the membrane-electrode assembly (MEA), non-uniform temperature, degree of humidification and configuration of the flow channels [4, 7]. Among these factors, cathode flooding is perhaps the most critical issue which significantly affects the cell performance.

Under flooding conditions, the pores of the cathode gas distribution layer, GDL, are filled by liquid water, partially or completely, blocking the transport of oxygen to the reaction sites, resulting in a non-uniform current distribution across the cell and serious performance drop, particularly at high current densities [8, 9]. Therefore, it is very important to understand the effect of water flooding on the local current distribution for designing and operating a PEM fuel cell.

Although many experimental and numerical studies have been published concerning the local current distribution in PEM fuel cells [7, 10-15], the effect of water flooding on the variations of local current density has received little attention. One of the most appealing research works was conducted recently by Liu *et al.* [16]. They studied membrane hydration and electrode flooding by developing a 2-D partial flooding model in which size distributions are assigned for the hydrophobic and hydrophilic pores of the GDL. The liquid water produced is considered to condense in hydrophilic and hydrophobic pores in sequence if the water vapor pressure is higher than the condensation pressure for the pores. The model results, under a wide range of operating conditions, have shown reasonable agreement with the experimental data.

The goal of this research is to add to the knowledge base and produce generic design guidelines for operating conditions and flow-fields that can be applied to PEM fuel cells undergoing cathode flooding. It is assumed that the development of these design techniques could be a useful tool for the improvement of water management, and shed further light on its effect on fuel cell performance. To this end, partially flooded GDL models are proposed to investigate the performance of a PEM fuel cell under

A. Jamekhorshid was with the School of Chem. and Petrol. Eng., Shiraz University, Shiraz, Iran. He is now with the Chem. Eng. Dept., Faculty of Eng., Tarbiat Modares University, Tehran, Iran (corresponding author, E-mail: a.jamekhorshid@modares.ac.ir; jamekhorshid@gmail.com; phone: +989173786898).

G. Karimi is Assistant Prof. in the School of Chem. and Petrol. Eng., Shiraz University, Shiraz, Iran (E-mail:ghkarimi@shirazu.ac.ir).

I. Noshadi is with the Faculty of Chemical & Natural Resources Eng., Universiti Teknologi Malaysia, UTM Skudai, Johor, Malaysia (E-mail: imannoshadi@gmail.com).

A. Jahangiri is with the Chem. Eng. Dept., Faculty of Eng., Tarbiat Modares University, Tehran, Iran (E-mail: jahangiri@ modares.ac.ir).

cathode flooding conditions and to determine how the local current density will be affected. The model was solved to obtain the variations in local current density along the cell flow fields over a wide range of cell operating conditions.

II. Model Development

A. Model Description

Fig. 1 shows a schematic diagram of a typical PEM fuel cell. As illustrated, a single cell, referred to as membrane electrode assembly (MEA), is composed of a membrane electrolyte sandwiched in the middle of the cell, and typically contains catalyst and microporous GDLs. One of the GDLs is referred to as the anode, the other as the cathode. The catalyst layer at the anode separates hydrogen molecules into protons and electrons. The membrane permits ion transfer (protons), requiring the electrons to flow through an external circuit before recombining with protons and oxygen at the cathode to form water. This migration of electrons produces useful work.

In practice, oxygen, pure or in air, enters the cathode side of the cell through an inlet and is distributed into the flow channels or fields. From the flow fields, O_2 diffuses through the GDL towards the cathode-membrane interface where it is reduced to form water and heat which are then removed from the system. Water can also be added to the cathode side due to the electroosmotic drag and be transferred from the cathode to the anode due to back diffusion.

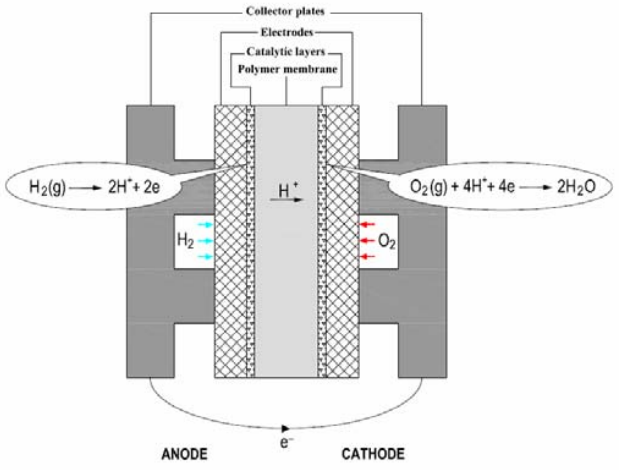

Fig. 1 Schematics of a PEM fuel cell

The simultaneous water and oxygen transfer, in conjunction with significant pressure variations in the cathode flow channels can lead to situations where the excess water in the cathode may fill the pore network within the GDL and decrease the effective diffusivity of oxygen through the layer. This phenomenon, known as water flooding, degrades the cell performance.

The modeling of liquid water and species transport in GDL is very complicated, due to different properties of pores, such as diameter, hydrophobicity, and etc. Although the topic has received considerable attention in recent years, only a few models addressed directly on simultaneous liquid and gas transport in porous GDL [16, 17].

In general, modeling of two-phase transport in gas diffusion layer is performed considering two distinct pore characteristics in GDL; they can be classified as (a) continuous or homogeneous model and (b) pore-scale method. Most of the existing models belong to the first approach, wherein average porosity, permeability, pore diameter and hydrophobicity are assigned to the homogeneous gas distribution layer [8, 18]. Based on this model, there are no preferred sites for water condensation. Therefore, water flooding, if any, starts from the catalyst layer and grows uniformly inside the GDL as illustrated in Fig. 2.a [19, 20]. Under this approach, the thickness of flooded region should not be large because of the presence of a continuous water film at the catalyst-GDL interface which blocks oxygen diffusion towards the reaction sites. As a result, local current densities at flooded regions should drop appreciably [21].

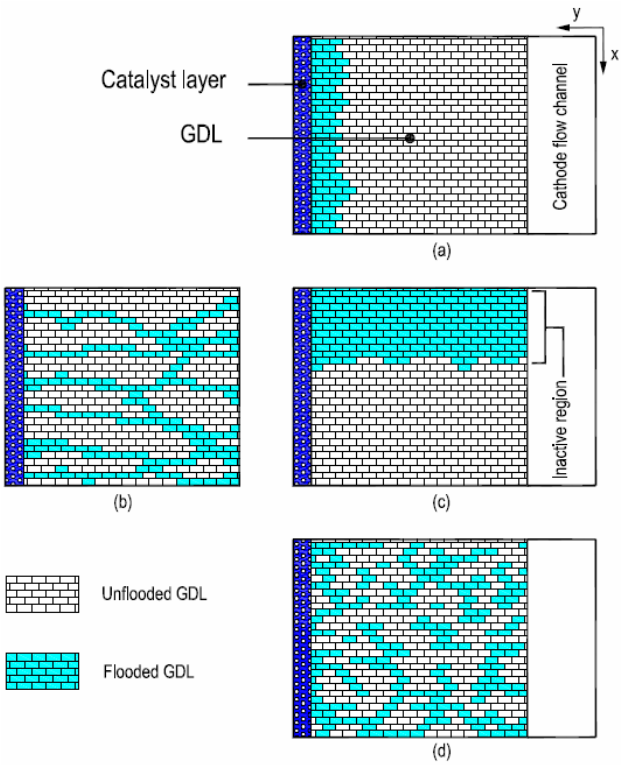

Fig. 2 Various models of GDL flooding; (a) Continuous model, (b) Pore-scale model, and (c) Volume-effective model

Pore-scale approach on the other hand, takes distributions in GDL pore size and hydrophobicity into account and seems to be helpful in understanding of transport phenomena in fuel cells. Notable contribution to the development of this approach has been made by Liu *et al.* [16]. Except for very high flooding rates, portions of catalyst layer are always available for O_2 reduction. In pore-scale approach, as illustrated in Figs. 2.b and c, GDL can be divided into two regions; an inactive (flooded) region through which oxygen diffusion is almost zero, and an active (unflooded) region where O_2 diffusion can occur. Therefore, until the entire pore networks are flooded with liquid water, oxygen can diffuse through the GDL and complete blockage of oxygen does not occur and reduction in current density is gradual.

In the present study, we introduce a third approach,

referred to as volume-effective approach, in which partial flooding occurs uniformly throughout the entire GDL as depicted in Fig. 2.d. As pores are occupied with liquid water, the pore properties including porosity and permeability are reduced and as a result, O_2 penetration is affected. Typical concentration profiles across the GDL for three approaches are shown in Figs. 3.a-c. In the present work, the three approaches are used to predicting the extent of flooding in the cathode side of PEM fuel cell. A comparison of the approaches is also performed.

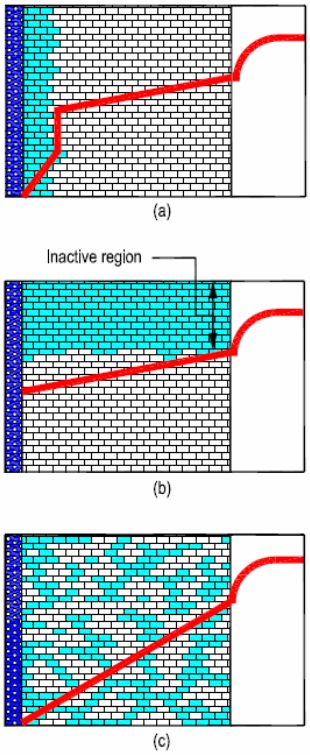

Fig. 3 Profiles of oxygen concentration across the cathode side of a PEM fuel cell; (a) Continuous model, (b) Pore-scale model, and (c) Volume-effective model

B. Species Transport

Two-dimensional, partially flooded GDL models presented here are based on the following assumptions: (a) Oxygen reduction occurs in the catalytic layer with negligible thickness. (b) The cell operates at constant temperature. (c) The gas mixtures are considered to be ideal. (d) The fuel cell operation is assumed to be steady-state. In addition, to make the analysis simple, anode and cathode flow fields are considered to have serpentine topology with fuel and oxidant flow parallel to each other.

Under steady-state condition, the rate of species transport from the flow channels to the reaction sites will determine the local current density. This transport however, is dependent on the mass transfer resistances in the flow fields and the flooded and unflooded segments of GDL. At a local position along the flow channel, x, conservation equations can be used to relate the rate of production of various species to the local current density, $I(x)$:

$$\frac{dN_i}{dx} = \xi_i \frac{wI(x)}{4F} \tag{1}$$

Anode channel: $\xi_{H_2} = -2,\ \xi_{H_2O,a} = -4\alpha$

Cathode channel: $\xi_{O_2} = -1,\ \xi_{H_2O,c} = 2 + 4\alpha,\ \xi_{N_2} = 0$

here, α denotes the net water drag coefficient (electroosmotic drag - back diffusion); meaning that there will be α moles H_2O transport from anode to cathode together with 1.0 mole H^+. The net water drag coefficient can be calculated from [22]:

$$\alpha = n_d - 100\frac{F}{I(x)} D_w \frac{c_{w,c} - c_{w,a}}{t_m} \tag{2}$$

where n_d, D_w, and t_m are the electroosmotic coefficient (= number of water molecules carried by a proton), diffusion coefficient of water in the membrane, and the membrane thickness, respectively. This electroosmotic coefficient depends on the water content in the membrane, which in turn depends on the activity of water in the gas phase next to the membrane. Expressions given by Springer *et al.* (1991) are used to calculate n_d and D_w as follows [23]:

$$n_d = \begin{cases} 0.0049 + 2.024a_a - 4.53a_a^2 + 4.09a_a^3 & a_a \le 1 \\ 1.59 + 0.159(a_a - 1) & a_a > 1 \end{cases} \tag{3}$$

$$D_w = n_d D^0 \exp\left[2416\left(\frac{1}{303} - \frac{1}{T}\right)\right] \tag{4}$$

Water concentration at the anode- and cathode-electrolyte interfaces can be calculated from [22]:

$$c_{w,k} = \begin{cases} \frac{\rho_{m,dry}}{M_{m,dry}}(0.043 + 17.8a_k - 39.85a_k^2 + 36.0a_k^3) & a_k \le 1 \\ \frac{\rho_{m,dry}}{M_{m,dry}}[14 + 1.4(a_k - 1)] & a_k > 1 \end{cases} \tag{5}$$

where the subscript k denotes either the anode or cathode. The activity of water in the anode and cathode streams is defined as follows:

$$a_c = \left(\frac{N_{H_2O,c}}{N_{H_2O,c} + N_{O_2} + N_{N_2}}\right)\frac{P_c}{P^{sat}} \tag{6}$$

$$a_a = \left(\frac{N_{H_2O,a}}{N_{H_2O,a} + N_{H_2}}\right)\frac{P_a}{P^{sat}} \tag{7}$$

C. Electrochemistry

The output voltage of a single cell can be determined by subtracting the overpotentials from the open circuit voltage as:

$$E_{cell} = E_{oc} - \eta_{act} - \eta_{ohm} \tag{8}$$

where [24]:

$$E_{oc} = 1.229 - 0.85\times10^{-3}(T - 298.15) + 4.31\times10^{-5}T[\ln P_{H_2} + \frac{1}{2}\ln P_{O_2}] \tag{9}$$

With anode overpotential neglected, the cathode overpotential can be calculated from [22]:

$$\eta_{act}(x) = \frac{RT}{0.5F}\ln\left(\frac{I(x)}{(1-f)I_0 P_{O_2}^{cat}}\right) \tag{10}$$

where I_0 is the exchange current density at a reference pressure and f is the fraction of flooded catalytic surface, where:

$$\begin{array}{ll} \textit{Continuous/volume-effective models:} & f = 0 \\ \textit{Pore-scale model:} & 0 \le f \le 1 \end{array} \quad (11)$$

Assuming ideal gas mixture, $P_{O_2}^{cat}(x)$ can be calculated from:

$$P_{O_2}^{cat}(x) = c_{O_2}^{cat}(x) RT \quad (12)$$

The O_2 concentration at the catalyst surface, $c_{O_2}^{cat}(x)$, is related to the O_2 concentration in the flow channels, $c_{O_2}^{bulk}(x)$, as follows [19]:

Flooded section:

$$c_{O_2}^{cat}(x) = \frac{RT}{H_{O_2}} c_{O_2}^{bulk}(x) - \frac{I(x)}{4F} \times \left[\frac{RT}{H_{O_2}} \left(\frac{1}{h_{O_2}} + \frac{[1-\varepsilon(x)]t_{GDL}}{D_{O_2\text{-g}}^{eff}} \right) + \frac{\varepsilon(x) t_{GDL}}{D_{O_2\text{-l}}^{eff}} \right] \quad (13)$$

Unflooded section:

$$c_{O_2}^{cat}(x) = c_{O_2}^{bulk}(x) - \frac{I(x)}{4F} \left(\frac{1}{h_{O_2}} + \frac{t_{GDL}}{D_{O_2\text{-g}}^{eff}} \right) \quad (14)$$

Equation (14) is valid for unflooded sections of all models, while (13) is only useful for flooded sections of continuous model. In (13), $\varepsilon(x)$ is the fraction of GDL flooded and defined as:

$$\varepsilon(x) = \frac{t_f}{t_{GDL}}, \; t_f = \frac{(P_{H_2O,c} - P_{H_2O,c}^{sat}) t_{GDL} Mw_{H_2O} \times 10^{-3}}{RT \rho_{H_2O} \varphi_0} \quad (15)$$

Here t_f is the thickness of liquid layer in continuous model. Bernardi and Verbrugge (1992) proposed the following correlation for Henry's constant [25]:

$$H_{O_2} = 0.1033 \exp\left(14.1 - \frac{666}{T}\right) \quad (16)$$

An effective diffusion coefficient, D^{eff}, must be used to determine O_2 transfer inside the GDL, whether flooded or unflooded; Bruggeman equation relates D^{eff} to GDL porosity, φ, as follows [23]:

$$D^{eff} = D(\varphi)^{3/2} \quad (17)$$

where φ varies for volume-effective model as GDL void fractions change with the extent of flooding as follows:

$$\varphi = \frac{A_{GDL} t_{GDL} \varphi_0 - V_{H_2O,l}}{A_{GDL} t_{GDL}} \quad (18)$$

where:

$$V_{H_2O,l} = \frac{(P_{H_2O,c} - P_{H_2O,c}^{sat}) t_{GDL} dA \varphi_0 Mw_{H_2O} \times 10^{-3}}{RT \rho_{H_2O}} \quad (19)$$

According to the (15) and (19), the well known liquid water saturation parameter, s, can be calculated as:

$$s(x) = \varepsilon(x) \times \varphi_0 \quad (20)$$

where it defined as the volume fraction of the total void space of GDL occupied by the liquid phase. Ideal gas law is used to calculate the oxygen concentration in the flow channels:

$$c_{O_2}^{bulk}(x) = \frac{P_{O_2}}{RT} \quad (21)$$

The O_2 mass transfer coefficient, h_{O_2}, can be estimated by considering mass transfer in a fully developed laminar flow through a three-sided adiabatic square duct with constant mass flux applied at one surface [26]:

$$\mathrm{Sh} = \frac{h_{O_2} d_h}{D_{O_2\text{-g}}} = 2.7 \quad (22)$$

where d_h is the channel hydraulic diameter. The O_2 diffusion coefficient in the cathode air stream is calculated from [27]:

$$D_{O_2\text{-g}} = \frac{1 - y_{O_2}}{\dfrac{y_{N_2}}{D_{O_2-N_2}} + \dfrac{y_{H_2O,c}}{D_{O_2-H_2O(g)}}} \quad (23)$$

where:

$$D_{O_2\text{-l}} = D_{O_2\text{-l}}^{std} \left(\frac{T}{298} \right)$$

$$D_{O_2-H_2O(g)} = D_{O_2-H_2O(g)}^{std} \left(\frac{T}{273} \right)^{2/3} \left(\frac{1}{P_c} \right)$$

$$D_{O_2-N_2} = D_{O_2-N_2}^{std} \left(\frac{T}{273} \right)^{2/3} \left(\frac{1}{P_c} \right) \quad (24)$$

The Ohmic overpotential associated with the membrane is calculated from [22]:

$$\eta_{ohm}(x) = 0.01 I(x) \frac{t_m}{\sigma_m(x)} \quad (25)$$

where the membrane conductivity, σ_m, is a function of the membrane water content at the anode interface:

$$\sigma_m = \left(0.00514 \frac{M_{m,dry}}{\rho_{m,dry}} c_{w,a} - 0.00326 \right) \times \exp\left(1268 \left(\frac{1}{303} - \frac{1}{T} \right) \right) \quad (26)$$

The average current density of the fuel cell at a specified voltage value could be calculated by integrating *I(x)* along the whole length of the flow channel:

$$I_{ave} = \frac{1}{l} \int_0^l I(x) dx \quad (27)$$

D. Solution Procedure

For the solution of PEM fuel cell governing equations, two options are available, namely, keeping constant average current density or keeping constant voltage. The authors adopted the latter in this work.

Fig. 4 shows the flow chart of solution procedure. The model governing equations are solved at predefined cell voltage and cathode outlet pressure. The anode and cathode flow fields are divided into a number of equally-sized segments and an average cell current density, I_{ave}, and a cathode inlet pressure are assumed. The anode inlet pressure is taken to be the same as that of cathode. The inlet molar flow rates (and mole fractions) for the fuel and oxidant streams are calculated based on I_{ave} and cell geometry.

Calculations are started from the first segment for which a local current density is also assumed. Variations in the species molar flow rates for the first segment are calculated from (1) and the segment voltage is estimated from (8) after open circuit voltage and overpotentials are calculated. If the calculated voltage differs from the predefined value, the assumed local current density should be corrected otherwise, calculations proceed to the next segment. This procedure is repeated until the calculations for the whole channel length is completed. At this point, the calculated cathode outlet pressure is compared with the assumed pressure. If there is a difference between the two, the inlet pressure must be corrected. In addition, the calculated I_{ave} is compared with the assumed value and if the convergence criterion does not meet, the initial guess for I_{ave} needs to be modified.

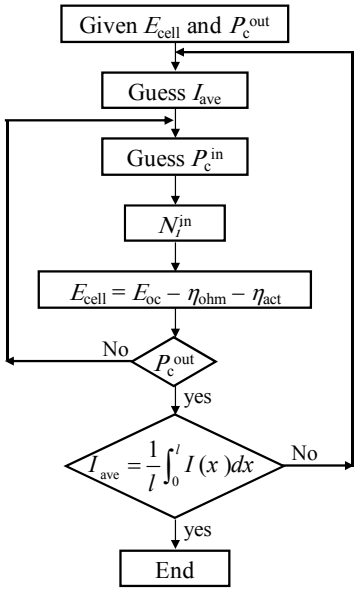

Fig. 4 Flow chart of solution procedure

III. Results and Discussions

The input parameters for the fuel cell are classified as design and operating parameters. Table I lists a summary of the operating and relevant design parameters used in the present study.

Fig. 5 shows variations in the local current density along the flow fields as predicted by continuous and pore-scale models. As expected, local current density starts from a maximum value at the cell inlet where excess amounts of the reactants at high local pressures exist. The current density then drops along the flow channels as the reactants are consumed and local pressure is decreased. As O_2 reduction proceeds along the cathode flow channels, air water content is expected to rise and the probability of cathode flooding increases. Cathode flooding should be initiated at the membrane-catalyst interface and grow inside the GDL towards the flow channels. Under cathode flooding, O_2 diffusion through GDL is expected to drop and results in a lower current density. The predicted fall in local current density could be abrupt or gradual depending on flooding model being used. With continuous model, all oxygen pathways to the catalyst layer are blocked with a thin water film. Hence, the local current density should

TABLE I
Parameters and Properties Used in the Present Partial Flooding Model

Component	Parameter	Value
Cell:	E_{cell}	0.5 V
	I_0	100 A/m^2
	T	323-368 K
	P_c^{out}	1.0-2.5 atm
	RH_c^{in}	10-95 %
	RH_a^{in}	10-100 %
	S_c	1.2-2.5
	S_a	1.2-5.0
Bipolar Plate:	W	0.15 m
	H	0.15 m
	l	2 m
	w	1 mm
	b	1 mm
GDL:	t_{GDL}	250 μm
	φ_0	60 %
Membrane:	D^0	5.5×10^{-7} cm^2/s
	t_m	220 μm
	$M_{m,dry}$	1100 g/mol
	$\rho_{m,dry}$	2 g/cm^3

plunge suddenly. Numerical results predicted such a case at x/l=0.42. From this location forward, the local current density remains almost constant; this can be attributed to the constant liquid film thickness and constant O_2 concentration at the catalyst layer which prevail at such a low current density as shown in Fig. 6.

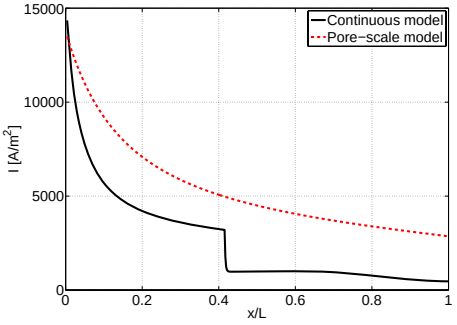

Fig. 5 Local current density distributions along the flow fields based on continuous and pore-scale models

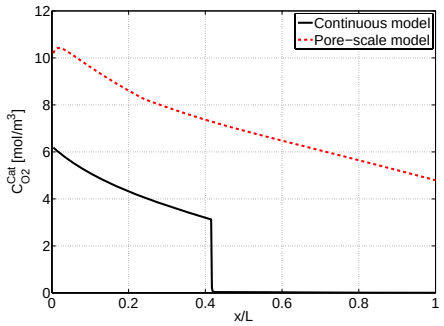

Fig. 6 Oxygen concentration distribution at catalyst layer along the flow fields based on continuous and pore-scale models

The complete blockage of oxygen pathways does not seem to be supported by experimental data. Therefore, either pore-scale or volume-effective approaches appear to

be more realistic. According to these models, there are always unflooded routes from the air channels towards the catalyst layer, allowing O_2 reduction, unless cathode GDL is entirely flooded with liquid water.

Figs. 7.a and b show how water activities vary along the anode and cathode sides of the cell as predicted by pore-scale and volume-effective models. As expected, along the cell, water activity decreases from 1 (fully saturated hydrogen) for the anode side due primarily to electroosmotic drag and increases for the cathode side due to water accumulation there. For the operating conditions presented in this figure, water activity at the cathode side exceeds one at a location of about x/l = 0.1 indicating the onset of cathode flooding.

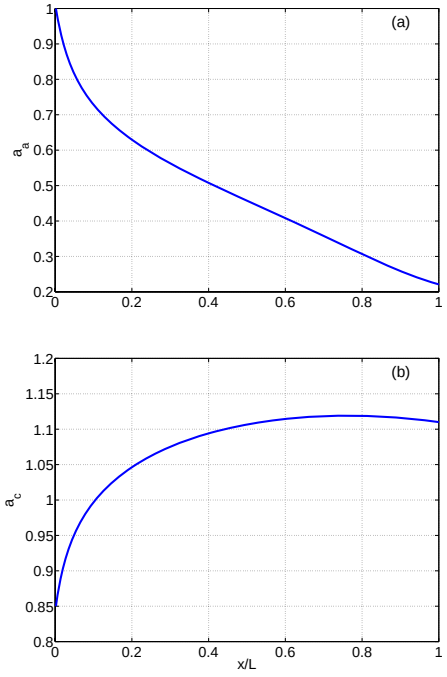

Fig. 7 Variations of (a) anode and (b) cathode water activities. (RH_c^{in} = 85%, RH_a^{in} = 100%, S_c = 1.75, S_a = 1.2, P_c^{out} = 1 atm, T = 353 K)

Variations in electroosmotic drag coefficient, n_d, and net water migration towards the cathode, α, are shown in Fig. 8. The difference between the two plots, $n_d - \alpha$, represents the amount of back diffusion from the cathode to the anode. This figure clearly indicates that in the entrance region, electroosmotic drag is dominant water transport mechanism across the membrane.

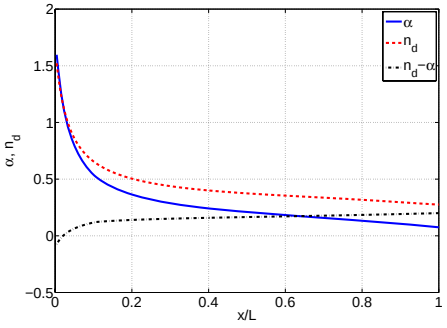

Fig. 8 Variations of water drag coefficients (RH_c^{in} = 85%, RH_a^{in} = 100%, S_c = 1.75, S_a = 1.2, P_c^{out} = 1 atm, T = 353 K)

The membrane conductivity, σ_m, is a strong function of anode water concentration as indicated in (26). Therefore, when water activity at the anode side is reduced, the membrane conductivity is expected to decrease, and so ohmic overpotential encounter with increment as displayed in Figs. 9.a and b. Beside, Fig. 9.b shows a decrease in ohmic overpotential that is due to the reduction of the current density (Fig. 9.c).

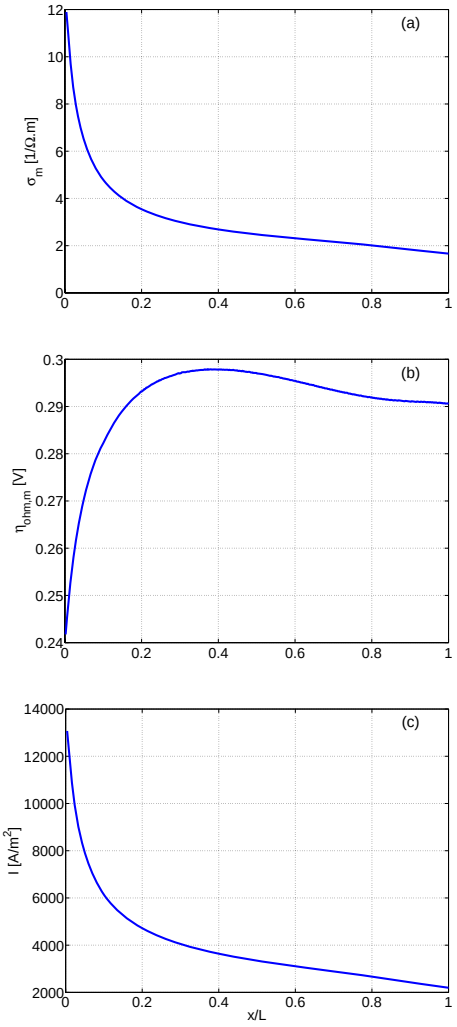

Fig. 9 Variations of (a) membrane conductivity, (b) ohmic overpotential, and (c) current density (RH_c^{in} = 85%, RH_a^{in} = 100%, S_c = 1.75, S_a = 1.2, P_c^{out} = 1 atm, T = 353 K)

During PEM fuel cell operation, it is critical to have an adequate water balance to ensure that the membrane remains hydrated for sufficient proton conductivity while cathode flooding and anode dehydration are avoided. Among various parameters involved, inlet relative humidities, stoichiometries, and cell operating temperature are most influential. In the following sections, the effect of these parameters, as predicted by pore-scale and volume-effective models, are discussed.

Figs. 10.a-c show how liquid water saturation, local current density and average current density vary along the channel at different levels of cathode humidification. As seen from Fig. 10.a, with an increase in RH_c^{in}, a larger portion of GDL volume is flooded with liquefied water and

a smaller catalyst surface area is accessible for O_2 reduction. As indicated in the figure, if $RH_c^{in} \leq 60\%$, no flooding occurs in the cell but for larger relative humidities cell experiences partial flooding. The larger the RH_c^{in}, the shorter the distance in which flooding is incepted. From fig. 10.b, it is seen that local current densities are degraded as the extent of flooding is augmented at high inlet humidities. Fig. 10.c shows that although increasing cathode inlet humidity will enhance the average current density for an unflooded cell ($RH_c^{in} \leq 60\%$), once flooding is started, a lower power output is attained. The models predict that there exists an optimal inlet humidity for which a maximum cell power can be obtained.

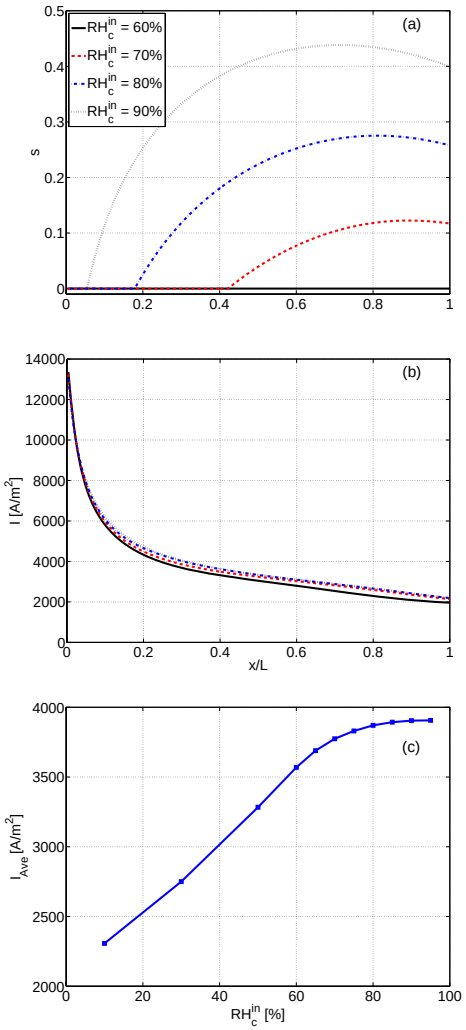

Fig. 10 Effect of cathode inlet humidity on (a) liquid water saturation, (b) local current density and (c) average current density (RH_a^{in} = 100%, S_c = 1.75, S_a = 1.2, P_c^{out} = 1 atm, T = 353 K)

Figs. 11.a and b show the effect of anode inlet relative humidity on extend of water flooding and local current density. As expected, although the lower anode inlet relative humidity would terminate the cathode flooding, due to membrane dehydration, the local current density and therefore the cell power will decrease.

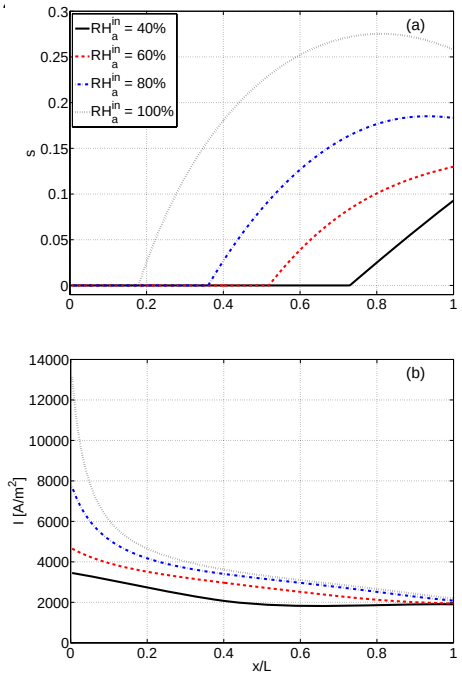

Fig. 11 Effect of anode inlet humidity on (a) liquid water saturation and (b) local current density (RH_c^{in} = 80%, S_c = 1.75, S_a = 1.2, P_c^{out} = 1 atm, T = 353 K)

Fig. 12 shows the effect of cathode stoichiometry, S_c, on the fraction of flooded GDL. As expected, at higher air flow rates larger amount of water can be removed from the cell. Therefore, cathode flooding can be delayed or even completely avoided. From these figure, it is seen that at RH_c^{in} = 60%, an S_c = 1.2 is more prone to flooding and $S_c \geq$ 1.8 prevent the cell form flooding as predicted by numerical models.

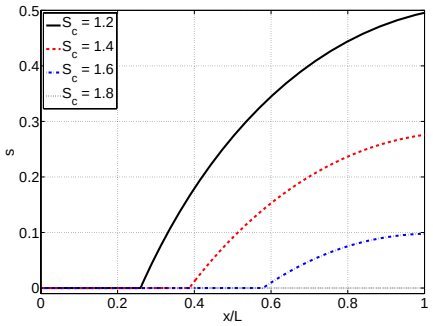

Fig. 12 Effect of cathode stoichiometry on liquid water saturation (RH_c^{in} = 60%, RH_a^{in} = 100%, S_a = 1.2, P_c^{out} = 1 atm, T = 353 K)

Fig. 13 shows that increasing cathode stoichiometry can improve the performance of a flooded cell by increasing the accessible catalyst surface area however, for an unflooded cell, larger stoichiometries would reduce membrane conductivity and lower average current density. So, there is an optimum cathode stoichiometry for which maximum power can be obtained.

The effect of anode stoichiometry on liquid water saturation and resulting local current density is illustrated on figs. 14.a and b. Increasing the anode stoichiometry is equal to higher hydrogen partial pressure that leads to elevated

local current density. Therefore, more water will produced at higher anode stoichiometry and so, the system will become more sensitive to flooding.

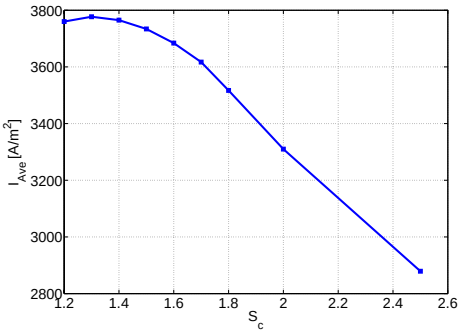

Fig. 13 Effect of cathode stoichiometry on the average current density (RH_c^{in} = 60%, RH_a^{in} = 100%, S_a = 1.2, P_c^{out} = 1 atm, T = 353 K)

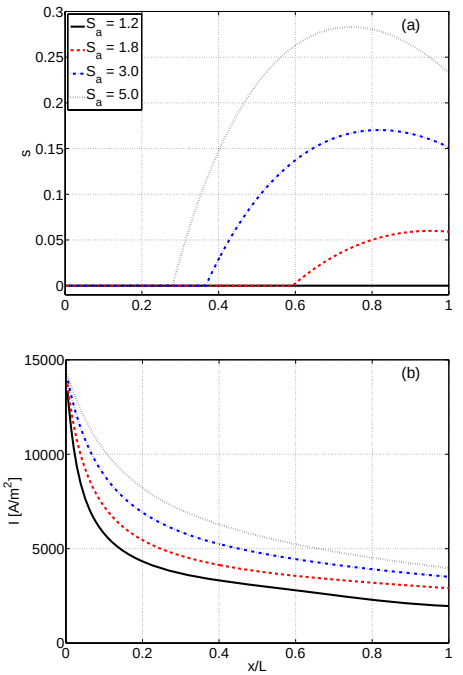

Fig. 14 Effect of anode stoichiometry on (a) liquid water saturation and (b) local current density
(RH_c^{in} = 60%, RH_a^{in} = 100%, S_c = 1.75, P_c^{out} = 1 atm, T = 353 K)

The effect of cell operating temperature on the state of flooding has been studied. Figs. 15.a and b show how raising cell temperature could prevent cell flooding and enhance its local current density.

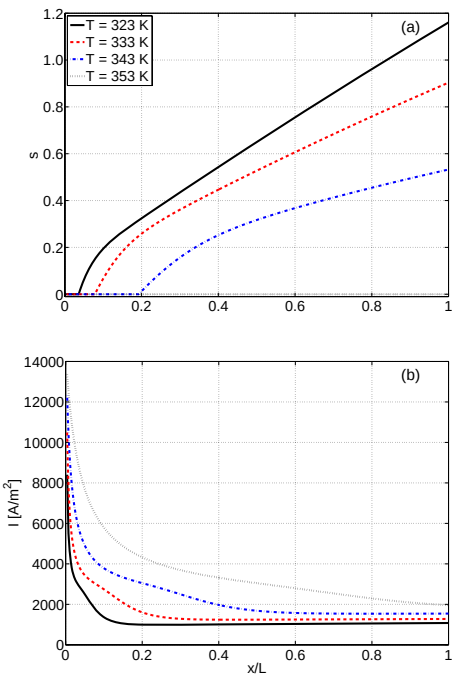

Fig. 15 Effect of cell temperature on (a) liquid water saturation and (b) local current density
(RH_c^{in} = 60%, RH_a^{in} = 100%, S_c = 1.75, S_a = 1.2, P_c^{out} = 1 atm)

IV. Conclusions

Many experimental and numerical studies have been performed over the past few years to asses the effects of variety of design and operating parameters on the local current distribution in PEM fuel cells. However, the effect of water flooding on the variations of local current density has received little attention. The present work examines the performance of a PEM fuel cell under cathode flooding conditions. Two-dimensional pore-scale and volume-effective approaches are proposed for the cathode side of PEM fuel cell based on conservation laws and electrochemical equations. The model results show a direct association between cathode inlet humidity increases and that of average current density but the system becomes more sensitive to flooding. The anode inlet relative humidity shows a similar effect. Operating the cell at higher temperatures would lead to higher average current densities and the chance of system being flooded is reduced. In addition, higher cathode stoichiometries prevent system flooding but the average current density remains almost constant. The higher anode stoichiometry leads to higher average current density and higher sensitivity to cathode flooding.

V. Acknowledgment

The financial support of the Renewable Energy Organization of Iran-SUNA is gratefully acknowledged.

References

[1] F. Barbir, *PEM Fuel Cells: Theory and Practice*. USA: Elsevier Academic Press, 2005.
[2] C. K. Dyer, "Fuel Cells for Portable Applications," *J. Power Sources*, vol. 106, pp. 31-34, 2002.
[3] J. J. Hwang, D. Y. Wang, and N. C. Shih, "Development of a Lightweight Fuel Cell Vehicle," *J. Power Sources*, vol. 141, pp. 108-115, 2005.

[4] S. J. C. Cleghorn, C. R. Derouin, M. S. Wilson, and S. Gottesfeld, "A Printed Circuit Board Approach to Measuring Current Distribution in a Fuel Cell," *J. Applied Electrochemistry*, vol. 28, pp. 663-672, 1998.
[5] J. J. Hwnag, W. R. Chang, R. G. Penng, P. Y. Chen, and A. Su, "Experimental and Numerical Studies of Local Current Mapping on a PEM Fuel Cell," *Int. J. of Hydrogen Energy*, vol. 33, pp. 5718-5727, 2008.
[6] F. B. Weng, A. Su, G. B. Jung, Y. C. Chiu, and S. H. Chan, "Numerical Prediction of Concentration and Current Distributions in PEMFC," *J. Power Sources*, vol. 145, pp. 546-554, 2005.
[7] C. Wieser, A. Helmbold, and E. Glzow, "A New Technique for Two-Dimensional Current Distribution Measurements in Electrochemical Cells," *J. Applied Electrochemistry*, vol. 30, pp. 803-807, 2000.
[8] J. J. Baschuk, and X. Li, "Modelling of Polymer Electrolyte Membrane Fuel Cells with Variable Degrees of Water Flooding," *J. Power Sources*, vol. 86, pp. 181-196, 2000.
[9] J. Larminie, and A. Dicks, *Fuel Cell Systems Explained*, John Wiley and Sons, 2003.
[10] A. Hakenjos, H. Muenter, U. Wittstadt, and C. Hebling, "A PEM Fuel Cell for Combined Measurement of Current and Temperature Distribution, and Flow Field Flooding," *J. Power Sources*, vol. 131, pp. 213-216, 2004.
[11] M. Noponen, T. Mennola, M. Mikkola, T. Hottinen, and P. Lund, "Measurement of Current Distribution in a Free-Breathing PEMFC," *J. Power Sources*, vol. 106, pp. 304-312, 2002.
[12] Y. G. Yoon, W. Y. Lee, T. H. Yang, G. G. Park, and C. S. Kim, "Current Distribution in a Single Cell of PEMFC," *J. Power Sources*, vol. 118, pp. 193-199, 2003.
[13] G. Bender, M. S. Wilson, and T. A. Zawodzinski, "Further Refinements in the Segmented Cell Approach to Diagnosing Performance in Polymer Electrolyte Fuel Cells," *J. Power Sources*, vol. 123, pp. 163-171, 2003.
[14] A. B. Geiger, R. Eckl, A. Wokaun, and G.G. Scherer, "An approach to measuring locally resolved currents in polymer electrolyte fuel cells," *J. Electrochem. Soc.*, vol. 151, pp. A394-A398, 2004.
[15] M. M. Mench, C. Y. Wang, and M. Ishikawa, "In Situ Current Distribution Measurements in Polymer Electrolyte Fuel Cells," *J. Electrochem. Soc.*, vol. 150, pp. A1052-A1059, 2003.
[16] Z. Liu, Z. Mao, and C. Wang, "A Two Dimensional Partial Flooding Model for PEMFC," *J. Power Sources*, vol. 158, pp. 1229-1239, 2006.
[17] J. J. Baschuk, and X. Li, "A general formulation for a mathematical PEM fuel cell model," *J. Power Sources*, vol. 142, pp. 134-153, 2004.
[18] G. Inoue, Y. Matsukuma, and M. Minemoto, "Effect of gas channel depth on current density distribution of polymer electrolyte fuel cell by numerical analysis including gas flow through gas diffusion layer," *J. Power Sources*, vol. 157, pp. 136-152, 2006.
[19] X. Li, *Principles of Fuel Cells*. New York: Taylor & Francis, 2006.
[20] G. Karimi, F. Jafarpour, and X. Li, "Characterization of flooding and two-phase flow in polymer electrolyte membrane fuel cell stacks," *J. Power Sources*, vol. 187, pp. 156-164, 2009.
[21] A. Jamekhorshid, G. Karimi, and X. Li, "Current Distribution in a Polymer Electrolyte Membrane Fuel Cell under Flooding Conditions," in *Proc. 7th Int. Fuel Cell Science, Engineering & Technology Conf.*, California, 2009.
[22] T. V. Nguyen, and R. E. White, "A Water and Heat Management Model for Proton-Exchange-Membrane Fuel Cells," *J. Electrochem. Soc.*, vol. 140, pp. 2178-2186, 1993.
[23] T. E. Springer, T. A. Zawodzinski, and S. Gottesfeld, "Polymer Electrolyte Fuel Cell Model," *J. Electrochem. Soc.*, vol. 138, pp. 2334-2342, 1991.
[24] C. L. Marr, "Performance Modelling of a Proton Exchange Membrane Fuel Cell," M.S. Thesis Dept. Mech. Eng., University of Victoria, Canada, 1996.
[25] D. M. Bernardi, and M. W. Verbrugge, "A Mathematical Model of the Solid-Polymer-Electrolyte Fuel Cell," *J. Electrochem. Soc.*, vol. 139, pp. 2477-2491, 1992.
[26] S. Kakac, R. S. Shah, and W. Aung, *Handbook of Single-phase Convective Heat Transfer*. New York: John Wiley and Sons, 1987, pp. 345-349.
[27] *Chemical Engineering Handbook*, 5th ed., McGraw-Hill, 1983.